BIOMOLECULES & THERAPEUTICS

Original Article
Biomol Ther 31(1), 27-39 (2023)

6-Shogaol and 10-Shogaol Synergize Curcumin in Ameliorating Proinflammatory Mediators via the Modulation of TLR4/TRAF6/MAPK and NFκB Translocation

Xian Zhou[1,*], Ahmad Al-Khazaleh[1], Sualiha Afzal[2], Ming-Hui (Tim) Kao[2], Gerald Münch[2], Hans Wohlmuth[1,3,4], David Leach[3], Mitchell Low[1] and Chun Guang Li[1,*]

[1]NICM Health Research Institute, Western Sydney University, Westmead, NSW 2145,
[2]School of Medicine, Western Sydney University, Campbelltown, NSW 2560,
[3]Integria Healthcare, Building 5, Freeway Office Park, QLD 4113,
[4]School of Chemistry & Molecular Biosciences, The University of Queensland, St Lucia, QLD 4072, Australia

Abstract

Extensive research supported the therapeutic potential of curcumin, a naturally occurring compound, as a promising cytokine-suppressive anti-inflammatory drug. This study aimed to investigate the synergistic anti-inflammatory and anti-cytokine activities by combining 6-shogaol and 10-shogaol to curcumin, and associated mechanisms in modulating lipopolysaccharides and interferon-ɣ-induced proinflammatory signaling pathways. Our results showed that the combination of 6-shogaol-10-shogaol-curcumin synergistically reduced the production of nitric oxide, inducible nitric oxide synthase, tumor necrosis factor and interlukin-6 in lipopolysaccharides and interferon-γ-induced RAW 264.7 and THP-1 cells assessed by the combination index model. 6-shogaol-10-shogaol-curcumin also showed greater inhibition of cytokine profiling compared to that of 6-shogaol-10-shogaol or curcumin alone. The synergistic anti-inflammatory activity was associated with supressed NFκB translocation and downregulated TLR4-TRAF6-MAPK signaling pathway. In addition, SC also inhibited microRNA-155 expression which may be relevant to the inhibited NFκB translocation. Although 6-shogaol-10-shogaol-curcumin synergistically increased Nrf2 activity, the anti-inflammatory mechanism appeared to be independent from the induction of Nrf2. 6-shogaol-10-shogaol-curcumin provides a more potent therapeutic agent than curcumin alone in synergistically inhibiting lipopolysaccharides and interferon-γ induced proinflammatory mediators and cytokine array in macrophages. The action was mediated by the downregulation of TLR4/TRAF6/MAPK pathway and NFκB translocation.

Key Words: Curcumin, Shogaol, Synergy, Anti-inflammatory, NFκB, TLR4/TRAF6/MAPK

INTRODUCTION

Infectious diseases are the leading cause of morbidity and mortality around the world (World Health Organization, 2020). As noted by mounting clinical observations, the mortality of infectious diseases is closely associated with the hyperactive immune response characterised by the excessive release of cytokines, interferons, and several other proinflammatory mediators, referred to as cytokine release syndrome (CRS) (Clark, 2007; Tisoncik *et al*., 2012; D'Elia *et al*., 2013; Chousterman *et al*., 2017; Soy *et al*., 2020; Wang *et al*., 2020; Meng *et al*., 2021).

CRS was firstly observed in influenza encephalopathy (Yokota, 2003), and subsequently found in variola virus infection (Jahrling *et al*., 2004), H5N1 influenza (Yuen and Wong, 2005), malaria cases (Clark, 2007), shigellosis (Islam *et al*., 2016), and COVID-19 (Coperchini *et al*., 2021). The latest research on COVID-19 confirmed the close link of CRS as the most dangerous event to COVID-19 pneumonia patients (Coperchini *et al*., 2021; Cron, 2021). Recent studies in

Open Access **https://doi.org/10.4062/biomolther.2022.039**

Received Mar 15, 2022 **Revised** Aug 11, 2022 **Accepted** Aug 18, 2022
Published Online Nov 2, 2022

***Corresponding Authors**
E-mail: c.li@westernsydney.edu.au (Li CG),
p.zhou@westernsydney.edu.au (Zhou X)
Tel: +61-2-9685-4743 (Li CG), +61-2-9685-4741 (Zhou X)
Fax: +61-2-9685-4760 (Li CG), +61-2-9685-4760 (Zhou X)

searching the appropriate targeting cytokine(s) against CRS have revealed that the onset of the host hyperinflammation involves multiple key cytokines and their interaction contributing to amplifying the response (Miossec, 2020) rather than a single cytokine target. For example, early clinical evidence suggested an elevated interleukin (IL)-6 level that associated with the severity of COVID-19 patients, however, using tocilizumab (IL-6 receptor blocker) monotherapy did not achieve a satisfactory clinical improvement in randomised clinical trials (Murthy and Lee, 2021). A single-centred, observational study reported the importance of IL-1 in the role of the survival rate of COVID-19, as evidenced by a significantly higher survival rate by using IL-1 (both IL-1α and IL-1β) inhibitor compared to that of using tocilizumab alone (Cron, 2021). Thus, it is evident that a combination immunomodulatory therapy with multi-targeted actions is more promising than a monotherapy to prevent or manage hyperinflammatory cytokines. The current treatment options of CRS are largely based on the use of steroids and non-steroidal anti-inflammatory drugs (NSAIDs). However, the action of NSAIDs is specific on cyclooxygenases but not pro-inflammatory mediators, and thus their efficacy is limited in addressing the CRS. In contrast, cytokine suppressive anti-inflammatory drugs (CSAIDs) aim to decrease a broad range of pro-inflammatory cytokines such as IL-1, IL-6, tumor necrosis factor-α (TNF), or nitric oxide (NO) (Soy *et al*., 2020) which may be more effective to combat CRS.

Multi-component therapeutics offer bright prospects for controlling complex diseases in a multiple targets approach, and their optimal therapeutic outcome is reached by two or more agents working together synergistically (Zhou *et al*., 2016). Synergy is defined as two or more agents reached a therapeutic outcome better than the sum of each individual agents (Zhou *et al*., 2016). Broadly, the synergy of two or more agents overcomes low efficacy and reduces side effects associated with high doses of single drugs, by reducing doses on each compound, or achieving context-specific multi-target mechanisms (Lehár *et al*., 2009).

Ginger (*Zingiber officinale* Roscoe) and turmeric (*Curcuma longa* L.) are well-known herbs that have been demonstrated to have health benefits in aiding inflammatory conditions. Our previous studies have demonstrated that ginger and turmeric extracts combined in a specific ratio of 5:2 (*w/w*) exhibited synergistic effects in inhibiting lipopolysaccharides (LPS) and interferon (IFN)-ɣ-induced proinflammatory mediators (Zhou *et al*., 2022a, 2022b). In addition, 6-shogaol (6-s), 10-shogaol (10-s) and curcumin (C) were identified as the leading compounds in reducing cytokines (Zhou *et al*., 2022a). Curcumin (C) has been extensively studied as the most promising therapeutic candidate of CSAIDs in attenuating proinflammation and CRS in bacterial and viral infections (Sordillo and Helson, 2015; Liu and Ying, 2020). The main mechanistic action of C in inhibiting proinflammatory cytokines was suggested by targeting the nuclear factor kappa B (NFκB) and induction of nuclear factor-erythroid 2-related factor 2 (Nrf2)/antioxidant response element pathways (Saw *et al*., 2010; Liu and Ying, 2020). However, the poor bioavailability of C have greatly affected its therapeutic outcome (Anand *et al*., 2007; Miao *et al*., 2016). On the other hand, 6-s and 10-s showed broad actions in suppressing proinflammatory mediators *via* downregulating the NFκB pathway, interfering p38 mitogen-activated protein kinase (MAPK) and upregulating Nrf2 (Pan *et al*., 2008; Chen *et al*., 2019). Notably, our previous study suggested that a combination of 6-s, 10-s and C equivalent to their ratio in ginger-turmeric (5:2, *w/w*) demonstrated the most potent nitric oxide inhibitory activity in LPS and IFN-γ-induced RAW 264.7 cells (Zhou *et al*., 2022a). Thus, it is speculated that 6-s and 10-s, the main bioactive components in ginger, help to further enhance the activity of C in CRS with a synergistic approach.

This study aimed to investigate the combined effect of 6-s, 10-s and C in reducing proinflammatory mediators and cytokines related to bacterial and viral infection. The synergistic interaction was aimed to be elucidated in the LPS and IFN-γ induced proinflammatory pathways to demonstrate the capacity of the combination as a more promising candidate for CRS than using C alone in infectious diseases.

MATERIALS AND METHODS

Preparation of chemical compounds

Chemical standards of 6-s, 10-s and C were purchased from Chengdu Biopurify Phytochemicals Ltd. (Chengdu, China; purity >98%). The identity and purity of standards were verified *via* high-performance liquid chromatography (HPLC) coupled with photodiode array detectors (Zhou *et al*., 2022a). The standard stock solutions of these reference compounds were prepared in dimethyl sulfoxide (DMSO) at the concentration of 10 mg/mL and stored at –20°C until use.

The preparation of the 6-s, 10-s and C mixture followed our previous study, of which the ratio was based on their quantity in the ginger-turmeric combination (5:2, *w/w*) (Zhou *et al*., 2022a). Briefly, 6-s and 10-s (S) was prepared by mixing these two compounds in DMSO at the ratio of 0.27:0.08, *w/w*. The combination of S and C (SC) was then prepared by mixing S and C according to the following ratio: 0.35:10.74, *w/w*. HPLC analysis for their quantities in ginger-turmeric extract (5:2, *w/w*) is shown in Supplementary Fig. 1 and Table 1. The final concentration of DMSO in S, C and SC was controlled to 0.1% in the media.

Cell lines and cell culture

The murine RAW 264.7 macrophages and stable human mammary MCF-7 AREc32 (AREc32) cells were kindly provided by Professor Gerald Münch in School of Medicine, Western Sydney University. Both cell lines were cultured at 37°C in Dulbecco's Modified Eagle Medium (DMEM, Lonza, Victoria, Australia) supplemented with 10% fetal bovine serum (FBS) (Life Technologies, Victoria, Australia), and 1% penicillin-streptomycin (Life Technologies) in a humidified atmosphere containing 5% CO_2 and 95% air.

Human monocytic THP-1 cells were purchased from ATCC (TIB-202™, Manassas, VA, USA) and maintained in RPMI 1640 (Lonza) supplemented with 10% FBS (Life Technologies), and 1% penicillin-streptomycin (Life Technologies) in a humidified atmosphere containing 5% CO_2 and 95% air.

Determination of proinflammatory cytokines

LPS from *Escherichia coli* 0111: B4 purified by trichloroacetic acid extraction (Sigma, Castle Hill, NSW, Australia) and IFN-γ (Lonza) were used to stimulate proinflammatory mediators including inducible nitric oxide synthase (iNOS), nitric oxide (NO), TNF and IL-6. RAW 264.7 cells (density at 1×10^6/mL) were seeded on 96-well cell culture plates (Corning Costar®, Sigma) and incubated for 48 h, followed by pre-treat-

ments with various samples. After the cells were incubated for 2 h, LPS and IFN-γ (both at 50 ng/mL) were added to the cells and co-incubated for another 18 h. After the stimulation, 100 μL of cells supernatant was collected and mixed with the Griess reagent (1% sulfanilamide in 5% phosphoric acid and 0.1% N-1-naphthylethylenediamine dihydrochloride in Milli-Q water) for the NO measurement. The plate with mixed supernatant and Griess reagent was monitored under 540 nm using a microplate reader (FLUORstar OPTIMA, BMG Labtech, Mornington, VIC, Australia). The rest of the cell supernatant was subjected to TNF and IL-6 ELISA assays using commercial ELISA kits (Lonza) according to the manufacturer's instructions. The absorbance was measured at 410 nm.

Human TNF and IL-6 levels modulated by various samples were tested using the human THP-1 cells. THP-1 cells (1×10^6/mL) were seeded in 96-well plate and differentiated by 50 nM of phorbol 12-myristate 13-acetate (PMA) overnight. The cells were treated with various samples for 2 h and stimulated with LPS (1 μg/mL). The cell supernatant was collected and subjected to TNF and IL-6 ELISA assays using commercial ELISA kits (Lonza) according to the manufacturer's instructions. The (3-(4,5-dimethylthiazol-2-yl)-2,5-diphenyltetrazolium bromide) tetrazolium reduction (MTT) and Alamar blue assays were used to measure the cell viability of RAW 264.7 cells and THP-1 cells, respectively.

Multiplex cytokine assay

THP-1 cells were seeded in a 24 well plate overnight and incubated with medium only, S (2.5 μg/mL), C (2.5 μg/mL) and SC (2.5 μg/mL) for 1 h followed by the stimulation of LPS (1 μg/mL) and human recombinant IFN-γ (50 ng/mL). After 24 h, the cell supernatant was collected and the total protein amount was determined by the Pierce BCA Protein Assay (Thermo Fisher Scientific, North Ryde, NSW, Australia). The cell viability was controlled by the Alamar blue assay. The equal amount of total protein collected from each sample was applied to the human XL Cytokine Array Kit (R&D Systems, Minneapolis, MN, USA) based on the manufacturers' protocol. Cytokines measured simultaneously (n=105) included but not limited to adiponectin/Acrp30, angiogenin, angiopoietin-1, angiopoietin-2, apolipoprotein A1, brain-derived neurotrophic factor, cluster of differentiation (CD)14, CD30, granulocyte colony-stimulating factor, intercellular adhesion molecule 1/CD54, IFN-ɣ, IL-1α, IL-2, IL-3, IL-4, IL-5, IL-6, IL-8, IL-10, IL-17A, and TNF.

Determination of Nrf2 activity by luciferase reporter assay

AREc32 cells (1×10^6 cells/mL) were seeded in 96 well plates and allowed for confluency overnight. The cells were then co-incubated with individual or combined S and C, medium only (blank control) and tert-Butylhydroquinone (tBHQ, positive control) for 24 h. The cell supernatant was then replaced with Alamar blue (0.01 mg/mL resazurin) for 1 h and the cell viability was examined with fluorescent absorbance under excitation 530 nm and emission at 590 nm using a microplate reader (FLUORstar OPTIMA, BMG Labtech, Mornington, VIC, Australia). The Alamar blue solution was then replaced with the triton lysis buffer (tris HCl: 1.71%, tris base: 0.51%, 5 M NaCl: 1.50%, 1 M MgCl2: 0.30%, Triton X 100 pure liquid: 0.75%) for the incubation of 10 min and placed in –20°C for another 20 min. The cell lysates were collected and transferred to a white micro-tire plate. The luciferin buffer was added to the cell lysates (D-luciferin 30 mg/mL: 0.53%, DTT 1 M: 3.00%, coenzyme A 10 mM: 1.50%, ATP 100 mM: 0.45%, 100 μL per well). The Nrf2 activity was measured by luminescence with an excitation of 488 nm and an emission of 525 nm. The induction of Nrf2 was determined by the fold change of the sample to that of the blank control.

Immunofluorescent staining on iNOS expression and NFκB nuclear translocation

RAW 264.7 cells were plated in the 8 well glass chamber at 20,000 cells/well overnight, and then co-incubated with 2.5 or 5 μg/mL of S, C, SC, 50 nM of brusatol (Bru, Nrf2 inhibitor, Sapphire Bioscience, Redfern, NSW, Australia), or vehicle (0.1% DMSO) in serum-free DMEM for 1 h prior to the stimulation of LPS (1 μg/mL). Cells were then washed with ice-cold phosphate-buffered saline (PBS) and fixed with 4% formaldehyde for 30 min at room temperature. Triton X 100 (0.1%) was used to permeabilize the cells for 20 min. Cells were then washed again with PBS three times and blocked by 1% bovine serum album (Sigma) for 1 h followed by overnight incubation at 4°C with mouse iNOS (1:100, Cell Signalling Technologies, Danvers, MA, USA) or mouse anti-p65 NFκB antibody (1:200, Santa Cruz Biotechnology, Dallas, TX, USA). Next, cells were washed with PBS and incubated with goat anti-mouse IgG conjugated with Alexa Fluor 488 green fluorescence (1:1,000) or Alexa Fluor 594 red fluorescence (1:1,000) both purchased from Thermo Fisher Scientific for 1 h in the dark room at room temperature. The chambers were then removed and the antifade mounting media with DAPI dye (blue color) was added before the imaging with the Zeiss LSM510 confocal microscope (Zeiss, Macquarie Park, NSW, Australia). Images were quantified and analysed using ImageJ (The National Institutes of Health and the Laboratory for Optical and Computational Instrumentation, Madison, WI, USA). Four different images were taken for each sample with two individual experiments. Over 10 representative cells were chosen randomly for analysis. The results were processed as the corrected total cell fluorescence corrected against the background (no fluoresce). The results were presented as corrected iNOS positive/negative expressions and nuclear fluorescence of % of nuclei positive p65 NFκB for each respective assay.

Determination of microRNA155-5p modulation by qPCR

RAW 264.7 cells treated with S, C and SC (2.5 μg/mL) were stimulated with LPS (1 μg/mL), and the total RNA was extracted by the mirVana miRNA isolation kit (Thermo Fisher Scientific). The total RNA (10 ng) was subjected to the reverse transcription using the TaqMan™ MicroRNA Reverse Transcription Kit (Thermo Fisher Scientific) performed on an Eppendorf Mastercycler EP Gradient S (Eppendorf, Macquarie Park, NSW, Australia). Then the cDNA samples were then prepared with TaqMan™ MicroRNA Assay (Thermo Fisher Scientific) before subjecting to the Mx3000/Mx3005P Real-Time PCR system (Stratagene/Agilent, Santa Clara, CA, USA). Each 20 μL reaction contained 10 μL SYBR Premix, 1 μL each primer, 1.33 μL cDNA and 7.67 RNase-free dH_2O. The cycling conditions shown as follows: step 1, 95°C for 20 s; step 2, 40 cycles at 95°C for 3 s and followed by 60°C for 30 s. Each assay was performed from three biological experiments and normalized to U6 RNA expression. The primer sequences for microRNA (miR)-155-5p and U6 RNA were obtained from Taq-

Man Thermo Fisher Scientific. The Comparative CT Method (ΔΔCT Method) was used to analyse the data to unravel the expression fold change between the treatments.

Western blot analysis on heme oxygenase-1 protein expression and LPS associated proinflammatory pathways

RAW 264.7 cells were grown in T75 cell flasks until confluency. Cells were then subjected to the treatments of S, C, SC (5 or 10 μg/mL), Bru (50 nM), with or without LPS (1 μg/mL) and incubated for various time points. Cells lysates were harvested and subjected to protein estimation by Pierce BCA Protein Assay (Thermo Fisher Scientific). Lysates were separated by SDS-PAGE electrophoresis (Bio-Rad, South Granville, NSW, Australia) and electro-transferred to a PVDF membrane (Thermo Fisher Scientific). The membranes were blocked in PBS-Tween 20 (0.1%) containing 5% skim milk powder for 20 min at room temperature, then incubated with the following primary antibodies overnight at 4°C: anti-iNOS (1:1,000, cat. no. 13120), anti-phospho JNK (1:1,000, cat. no. 4688), anti-JNK (1:1,000, cat. no. 9252), anti-phospho-c-Jun (1:1,000, cat. no. 32700), anti-c-Jun (1:1,000, cat. no. 9165), anti-Toll-like receptor 4 (TLR4, 1:1,000, cat. no. 14358), anti-tumor necrosis factor receptor associated factor 6 (TRAF)-6 (1:1,000, cat. no. 67591), anti-heme oxygenase-1 (HO-1, 1:1,000, cat. no. 26416). Beta-actin (1:1,000, cat. no. 4970) or GAPDH (1:1,000, cat. no. 5174) were used as the internal control. Following the membrane wash by PBST buffer (PBS with 1% tween 20), immunoreactive bands were detected by incubating with anti-rabbit (1:1,000, cat. no. 14708) or anti-mouse (1:1,000, cat. no. 14709) antibodies conjugated with horseradish peroxidase for 1 h. All the antibodies were purchased from Cell Signaling Technologies (Danvers, MA, USA). Immunoreactive bands were visualized by the Pierce™ ECL Western Blotting Substrate (Thermo Fisher Scientific). The intensity of the detected bands was analysed and quantified using ImageJ software.

Determination of synergistic interaction

The interaction in the combination was determined by combination index (CI) model based on the Chou-Talalay's method using the CompuSyn software 2.0 (ComboSyn, Paramus, NJ, USA). Synergy occurs when the CI value<1, whereas antagonism refers to CI value>1 (Zhou *et al*., 2016). In addition, the CI-Fa curve was generated which shows the dynamic change of the interaction in the combination (shown as CI values) with the default effect level (referred to as Fa value set between 0-100%) on a specific biological target. In our study, Fa values were referred to the suppressive responses on NO, IL-6 and TNF, respectively (Zhou *et al*., 2017, 2019).

Statistical analysis

All data were expressed as mean ± standard deviation (n≥3) and the difference among groups was analysed by GraphPad Prism 8 (Dotmatics, Boston, MA, USA) using one-way analysis of variances (ANOVA). *p* value less than 0.05 was considered as statistically significant.

RESULTS

SC synergistically attenuated LPS and IFN-γ-induced major proinflammatory cytokines

The combined activities of SC in inhibiting key proinflammatory cytokines in both RAW 264.7 and THP-1 cells were compared to that of S or C alone in order to determine the plausible synergistic interaction. MTT assay revealed that the tested concentrations of S, C and SC (0.34-22.10 μg/mL) on RAW 264.7 cells did not exhibit any significant cytotoxicity (Fig. 1A). Similarly, Alamar blue assay in THP-1 cells (Fig. 1B) suggested that SC S and C did not have any abvious cytotoxicity within the tested dosage range (0-22.10 μg/mL).

SC markedly reduced the expressions of TNF in both RAW 264.7 and THP-1 cells. In RAW 264.7 cells (Fig. 1C), SC (0.69-11.05 μg/mL) showed a dose-dependent inhibitory manner of TNF with the IC_{50} value of 6.63 ± 0.57 μg/mL which was much less than that of the IC_{50} values of C (8.69 ± 0.63 μg/mL) and S (9.97 ± 1.86 μg/mL). A similar trend was found in the THP-1 cells (Fig. 1D). SC showed the most significant inhibitory effect of human TNF with an IC_{50} value of 4.71 ± 0.77 μg/mL, which was slightly lower than that of C (IC_{50}=5.11 ± 0.76 μg/mL) and S (6.09 ± 1.02 μg/mL). CI-Fa curves in both murine and human TNF revealed that there was weak synergy at various effective ranges (Fig. 1E-1F) with synergy appeared at the lower level of tested concentrations in RAW 264.7 cells, whereas synergy at higher concentrations in THP-1 cells.

On the other hand, SC showed a strong synergy in reducing IL-6 in both RAW 264.7 and THP-1 cells (Fig. 1G-1J). S, C and SC all dose-dependently inhibited murine and human IL-6, and the most potent activity was shown in SC. The IC_{50} values of SC in reducing murine and human IL-6 were 2.37 ± 0.70 μg/mL and 1.45 ± 0.19 μg/mL, respectively, which were markedly lower than that of C (5.15 ± 1.22 and 2.13 ± 0.69 μg/mL) and S (2.95 ± 0.81 and 2.88 ± 1.16 μg/mL). CI-Fa curves suggested strong synergies in inhibiting IL-6 with CI values lower than 0.90 when Fa<0.86 in RAW 264.7 cells (Fig. 1H), and CI lower than 0.74 when 0.25>Fa>0.97 in THP-1 cells (Fig. 1J). This trend is similar to that in the inhibition of TNF.

SC showed a broader and greater anti-cytokine activity in LPS and IFN-γ-induced cytokine profiling assay using THP-1 cells

We have further explored the broad anti-cytokine activity of SC in comparison to S and C at the same concentration in LPS and IFN-ɣ induced multi-cytokine array assay in THP-1 cells. Typical cytokine images in cells pre-treated with S, C and SC and stimulated with LPS and IFN-ɣ are shown in Fig. 2A. Upon the activation of LPS and IFN-ɣ, a total of 25 cytokines were spotted (Fig. 2A, 2B) as evidenced by the obvious dot pixel density (each cytokine has two dots on the membrane as two replicates) detected by chemiluminescence. Among them, 9 cytokines displayed significant different expressions among groups, including CXCL-5, IL-6, IL-8 (CXCL8), CXCL10, CXCL11, TNF, monokine induced by gamma interferon (MIG), macrophage inhibitory cytokine-1 (MIC-1) and macrophage inflammatory protein 3α (MIP-3α). As shown in Fig. 2C, C (2.5 μg/mL) showed the down-regulatory trend for most of 9 cytokines except for CXCL11, with the significant inhibition on MIC-1 (p<0.05) and TNF (p<0.01). S only showed a significant inhibition in MIC-1 (p<0.05). Remarkably, SC exhibited the greatest inhibitory effects against all these cytokines, of

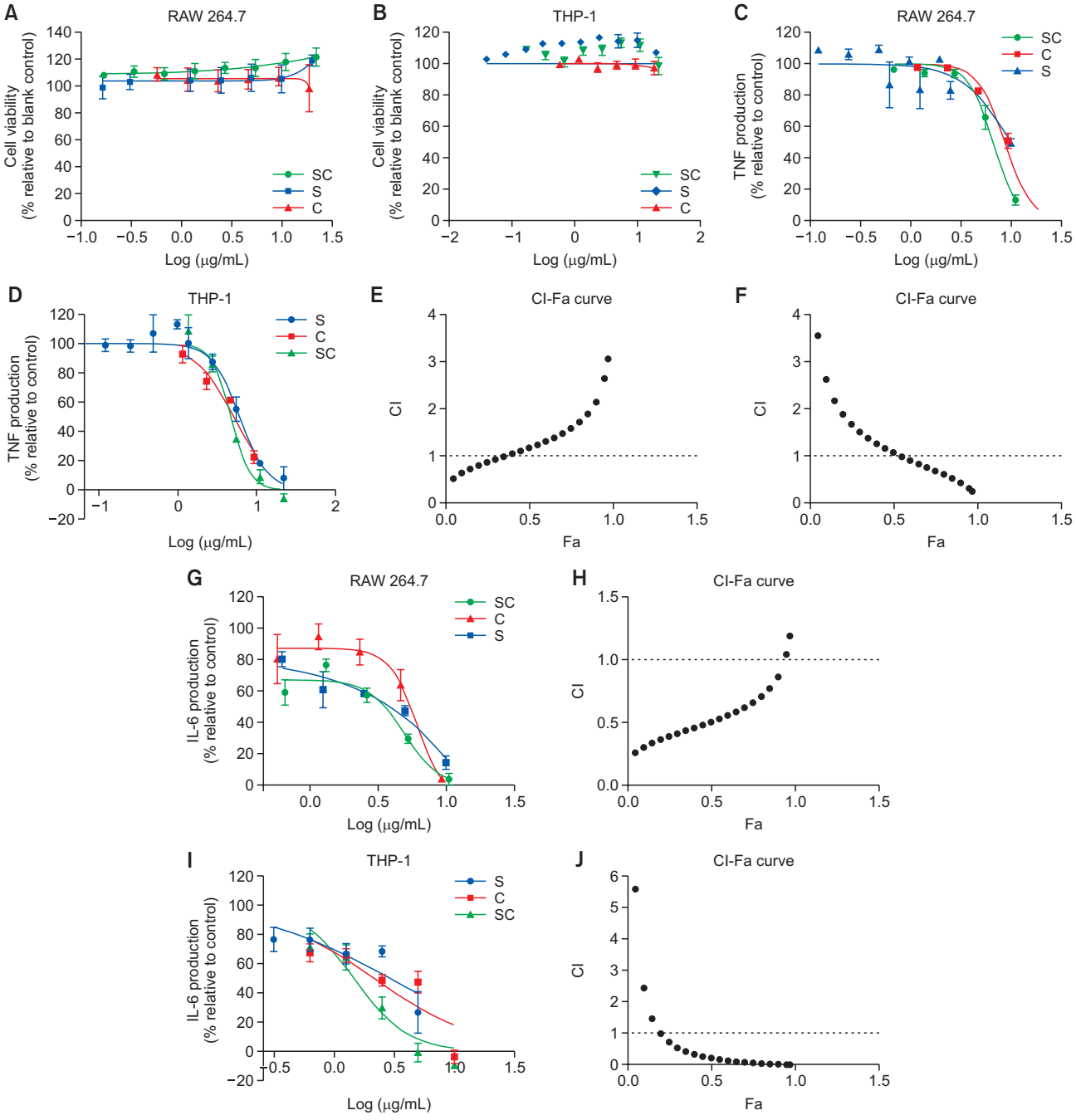

Fig. 1. SC synergistically reduced LPS and IFN-γ-induced TNF and IL-6 productions in murine RAW 264.7 and PMA-differentiated human THP-1 cell lines (n≥3 individual experiments). (A) Cell viability of RAW 264.7 cells treated by S, C and SC (0-22.10 μg/mL). (B) Cell viability of THP-1 cells treated by S, C and SC (0-22.10 μg/mL). Dose-response curves of S, C and SC in inhibiting TNF (C) and CI-Fa curve (D) in RAW 264.7 cells, and in THP-1 cells (E, F). Dose-response curves of S, C and SC in inhibiting IL-6 (G) and CI-Fa curve (H) in RAW 264.7 cells, and in THP-1 cells (I, J). The CI-Fa curves revealed the interaction (synergistic when CI<1 or antagonistic when CI>1) of SC at all TNF and IL-6 inhibitory levels (Fa values ranged from 0 to 1).

which the inhibition was significantly higher than that of C and S in CXCL5 (p<0.05 and p<0.01), MIC-1 (p<0.05 and p<0.01), IL-8 (p<0.05 and p<0.01), CXCL10 (both p<0.001), CXCL11 (p<0.0001 and p<0.01), MIP-3a (p<0.05 and p<0.01), MIG (p<0.05 and p<0.01) and TNF (p<0.01 and p<0.001).

SC synergistically inhibited LPS and IFN-γ-induced nitric oxide and iNOS protein expression

As shown in Fig. 3A, S, C and SC dose-depedndently inhibited NO expressions, and the IC_{50} value of SC (2.91 ± 0.20 μg/mL) was markedly lower than that of C (IC_{50}=6.16 ± 0.52 μg/mL) and S (IC_{50}=4.75 ± 2.57 μg/mL), suggesting a greater

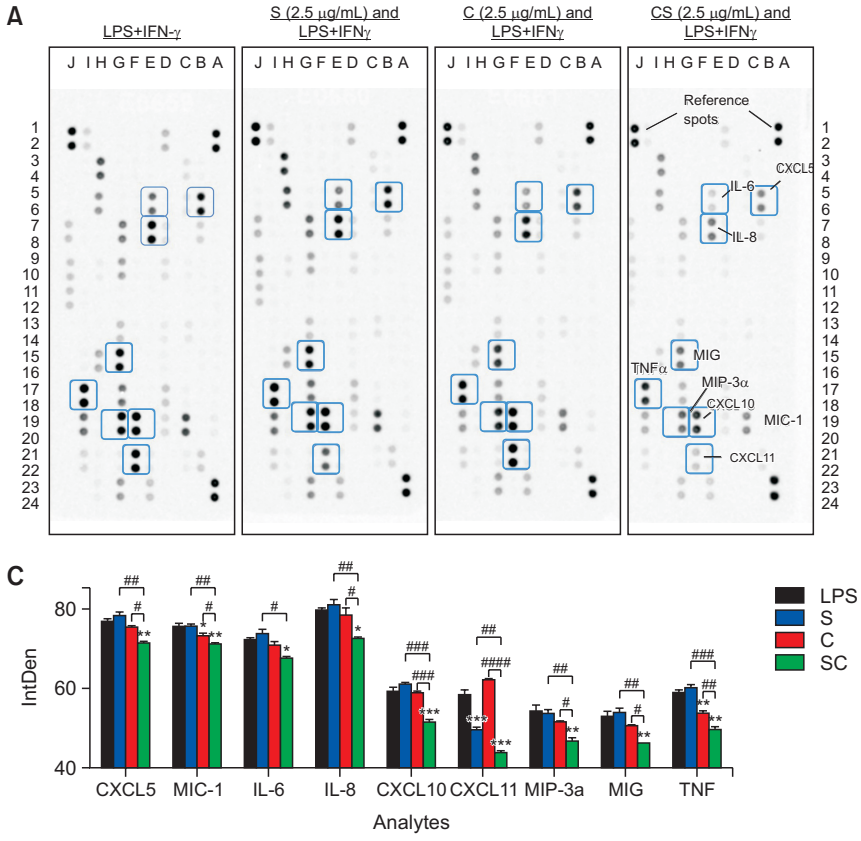

Coordinate	Analyte/control
A1,2	Reference spots
A23,24	Reference spots
B5,6	Chitinase 3-like 1
B7,8	Complement factor D
B21,22	EMMPRIN (CD147)
C3,4	ENA-78 (CXCL5)
C19,20	MIC-1
D1,2	CXCL1
D17,18	IL-1β
D19,20	IL-1ra
E5,6	IL-6
E7,8	IL-8
E23,24	IL-18 BPa
F19,20	CXCL10
F21,22	CXCL11
G7,8	MCP-1
G9,10	MCP-3
G13,14	MIF
G15,16	MIG
G17,18	MIP-1α/MIP-1β
G19,20	MIP-3α
G23,24	MMP-9
H3,4	Osteopontin
H5,6	PDGF-AA
H15,16	RANTES
I17,18	TNF-α
I19,20	uPAR

Fig. 2. SC showed a broader and stronger proinflammatory inhibition in cytokine microarray in human THP-1 cells. THP-1 cells (differentiated by 50 nM PMA) were treated with media, S (2.5 μg/mL), C (2.5 μg/mL) and SC (2.5 μg/mL), and stimulated with LPS (1 μg/mL) and IFN-ɣ (50 ng/mL) for 24 h. Four membranes were used to show activated cytokines treated by LPS and IFN- ɣ, pre-treated with S, C and SC (A). The list of activated cytokines is shown in (B). The semi-quantitative results are shown as averaged IntDen (n=2, each cytokine has two replicated dots) analysed by ImageJ (C). *p<0.05, **p<0.01, ***p<0.001 *vs.* LPS, $^{\#}p$< 0.05, $^{\#\#}p$<0.01, $^{\#\#\#}p$<0.001, $^{\#\#\#\#}p$<0.0001 *vs.* S or C.

potency. A very strong synergy was detected in reducing NO by SC with CI values in the range of 0.29 to 0.63 when Fa (NO inhibition)>0.1 as shown by the CI-Fa curve (Fig. 3B). A similar trend was observed in SC inhibiting iNOS expression as detected by the immunofluorescence. In Fig. 3C, most cells that have been activated by LPS (1 μg/mL) expressed iNOS green fluorescence with significantly higher (p<0.0001) the positive iNOS expression than that of the blank control (Fig. 3D). S, C and SC at 2.5 μg/mL significantly inhibited the iNOS expression with p<0.0001 *vs.* blank control. The most prominent activity was seen in SC, with the least iNOS positive cells observed, although no statistical significance was detected comparing SC to that of S and C alone. In Fig. 3E, Western blot analysis showed that SC at 5 μg/mL significantly reduced iNOS protein expression (p<0.05) compared to that of LPS stimulation, while S or C displayed a decreasing trend although the reductions were not significant.

Multi-targeted anti-inflammatory mechanism of SC related to the activation of Nrf2-HO-1 pathway

The mechanism of SC that synergistically reduced proinflammatory mediators was firstly explored in the action of Nrf2 activity, which serves an essential intracellular anti-oxidant and anti-inflammatory regulator.

Our results showed that SC, C and S dose-dependently induced the Nrf2 activity at high tested concentration range (Fig. 4A-4C). The maximum-induction of Nrf2 induced by SC was 13.27 ± 1.54 folds at 16.40 μg/mL without causing cytotoxicity, which the maximum induction was significantly higher than that of C (6.65 ± 0.36 folds at 9.26 μg/mL) and S (6.17 ± 1.00 folds at 10 μg/mL) (both p<0.05). The positive control, tBHQ (0.13–4.16 μg/mL), increased the luminescence signal of Nrf2 in a concentration-dependent manner (Fig. 4D) with the maximum Nrf2 activity of 11.45 ± 1.31 fold at 4.16 μg/mL. The CI-Fa curve and isobologram showed a synergistic interaction of SC in the activation of Nrf2 at all tested concentrations (Fig. 4E-4F). CI values were constantly lower than 1 at all Fa values (Nrf2 up-regulatory effect level), with CI values at 0.55, 0.57 and 0.60 at Fa 0.25, 0.5 and 0.75, respectively.

As shown in Fig. 4G, the 24 h's co-incubation of C (10 μg/mL) showed an increasing trend of HO-1 protein expression. Both S and SC (10 μg/mL) significantly increased HO-1 expression compared to blank (p<0.05). As expected, the co-incubation of Bru (Nrf2 inhibitor, 50 nM) in the RAW 264.7 cells (Fig. 4H) blocked the induction of HO-1 (p>0.05 *vs.* Blank). The co-incubation of Bru slightly impaired the HO-1 induction by SC, as evidenced by the significance of HO-1 induction by SC+Bru to a lesser degree (p<0.05) in comparison to SC only (p<0.01).

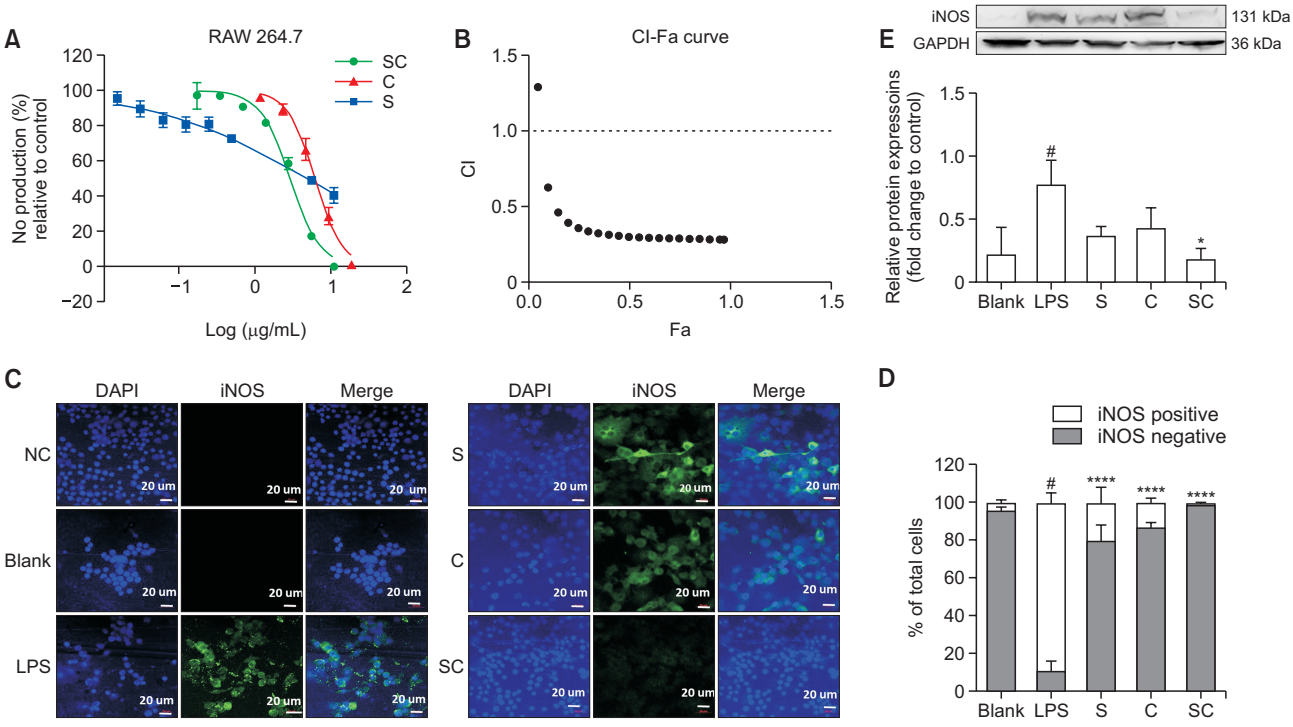

Fig. 3. SC synergistically reduced LPS and IFN-γ-induced NO production in murine RAW 264.7 cells (n≥3 individual experiments). (A) Dose-response curves of S, C and SC in inhibiting NO and (B) CI-Fa curve in RAW 264.7 cells. The CI-Fa curves revealed the interaction (synergistic when CI<1 or antagonistic when CI>1) of SC at all NO inhibitory levels (Fa values ranged from 0 to 1). (C) S, C and SC at 2.5 μg/mL inhibited LPS activated iNOS expression in the RAW 264.7 cells by immunofluorescence staining. Images were taken by a confocal microscope with 40x magnification. Blue: DAPI in the nucleus, green: iNOS in the RAW 264.7 cells. Scale bar=20 μm. (D) Statistical analysis of iNOS positive and negative fluorescence (% of total cells per image). $^{\#}p$<0.05 LPS *vs.* blank. ****p<0.0001 of iNOS positive compared with LPS. (E) Western blot analysis of iNOS total protein expression. RAW 264.7 cells were treated with medium only (Blank), LPS (1 μg/mL), S (5 μg/mL), C (5 μg/mL), and SC (5 μg/mL) for 24 h, and the total protein was lysed for Western blotting. $^{\#}p$<0.05 *vs.* Blank, *p<0.05 *vs.* LPS.

Multi-targeted anti-inflammatory mechanism of SC related to the feedback loop of NFκB nuclear translocation and miR-155-5p

In the absence of LPS, NFκB p65 was observed almost exclusively in the cytoplasm with DAPI blue in the nucleus and p65-fluor 594 red fluorescence outside the nucleus (Fig. 5A). However, the nuclear content of p65 increased dramatically following LPS (1 μg/mL) as indicated by the overlapping of p65-fluor 594 red fluorescence with the DAPI blue staining in the nucleus. The inhibitory effect of p65 translocation was compared among S, C and SC at 5 μg/mL. Our results in Fig. 5B showed that S did not inhibit p65 translocation, whereas C showed a significant inhibitory effect p<0.0001 compared to that of LPS. SC showed an apparent inhibitory activity in p65 translocation with prominent amounts of p65 expressed outside the nucleus. The statical analysis showed that the nuclear p65 localization was significantly reduced by SC (p<0.0001 *vs.* LPS), which the reduction was significantly greater than that of C (p<0.01) and S (p<0.0001).

The mechanism of SC in relation to NFκB mediated pathway was further explored in the expression of miR-155-5p which the overexpression amplifies the NFκB signalling induced proinflammation (Jablonska *et al.*, 2015). Three individual experiments were conducted to examine the modulatory effects of SC, S and C at 2.5 μg/mL on mmu-miR-155-5p (Fig. 5C). LPS (1 μg/mL) resulted in up to 123.62 ± 35.67-fold increase in mmu-miR-155-5p expression compared to blank control. It was noticed that S did not show a significant reduction of miR-155-5p (p>0.05). In contrast, both C and SC treatments substantially decreased the increased expression of 155-5p with statistical significances. In particular, SC showed the most significant inhibitory effects (p<0.001), which almost restored the level of 155-5p to a comparable level of untreated cells (blank).

In addition, the p65 translocation under SC (5 μg/mL) and Bru co-incubation was observed to see whether the blockage of Nrf2 exhibit any impact on the SC's modulation on NFκB signaling. As shown in Fig. 6A and 6B, LPS (1 μg/mL) triggered an accumulative amount of p65 into nucleus (p<0.0001) compared to that of the blank control, and the translocation was partially blocked by SC (p<0.01). An obvious p65 translocation (p<0.0001) was also observed in the cells treated with LPS (1 μg/mL) and Bru (50 nM). However, the translocation remained significantly inhibited by the treatment of SC even with the presence of Bru (p<0.0001), as compared to the treatments of LPS and LPS+Bru.

Multi-targeted synergistic mechanism of SC in inhibiting proinflammatory mediators related to the down-regulation of TLR4-TRAF6-MAPK signalling pathway

In order to further explore the synergistical mechanism of SC, the modulations of SC on LPS-mediated key proteins in

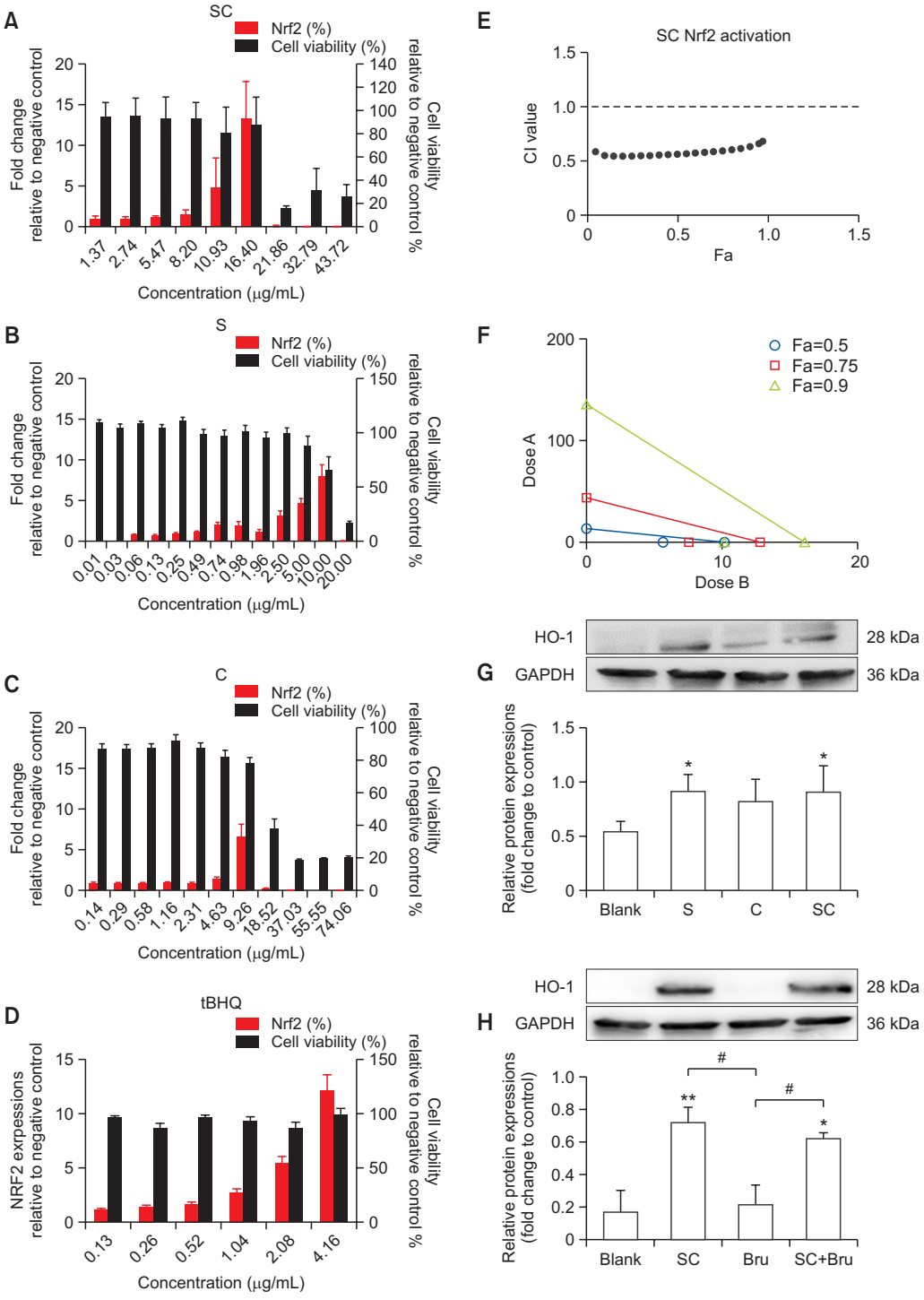

Fig. 4. SC synergistically induced Nrf2 activation as detected by luciferase assay. Dose-response curves of SC (A), C (B), S (C) and tBHQ (D) on Nrf2 activation and cell viability using AREc32 cells. All the data are presented as mean with SEM ($n \geq 3$ individual experiments). CI-Fa curve (E) and isobologram (F) revealed strong synergistic activity of SC in activating Nf2 total protein. CI<1 represents synergy. Fa represents the Nrf2 induction effect. (G) Western blot analysis of HO-1 total protein expression. RAW 264.7 cells were treated with medium only (Blank), S (10 μg/mL), C (10 μg/mL), and SC (10 μg/mL) for 24 h, and the total protein was lysed for Western blotting. *p<0.05 *vs.* Blank. (H) Western blot analysis of HO-1 total protein expression with the co-incubation of Nrf2 blockage (Bru). RAW 264.7 cells were treated with medium only (Blank), SC (5 μg/mL), Bru (50 nM), and SC (5 μg/mL)+Bru (50 nM) for 24 h, and the total protein was lysed for Western blotting. *p<0.05, **p<0.01 *vs.* Blank. $^{\#}p$<0.05 *vs.* Bru.

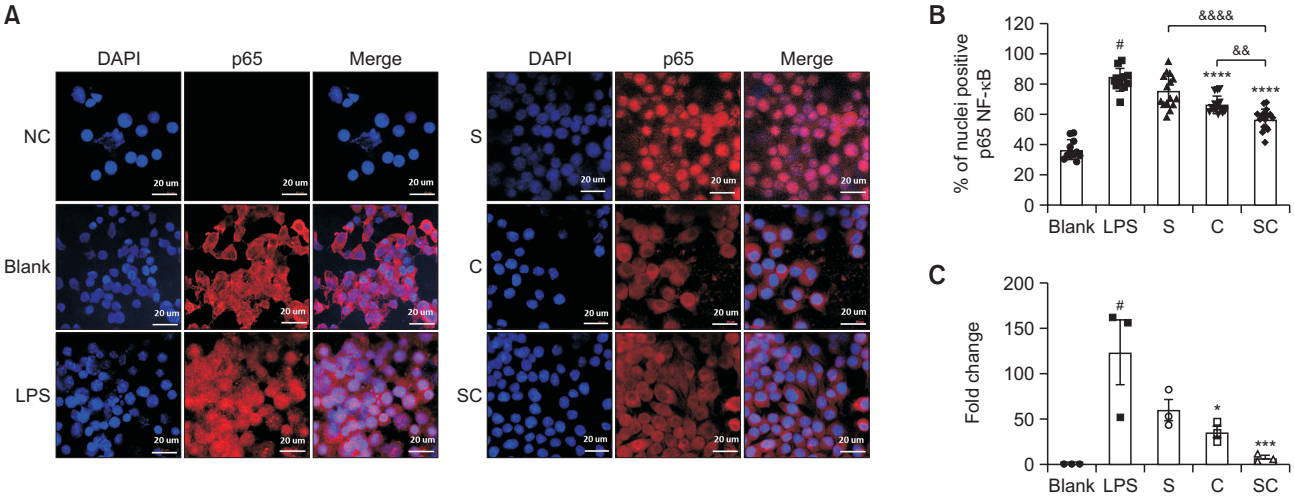

Fig. 5. SC reduced NFκB translocation and microRNA-155-5p expressions in LPS and IFN-γ-stimulated RAW 264.7 cells (n=3 individual experiments). (A) S, C, and SC at 5 μg/mL inhibited LPS activated NFκB p65 translocation in the RAW 264.7 cells by immunofluorescence staining. Images were taken by using a confocal microscope with 60x magnification. Blue: DAPI in the nucleus, red: NFκB p65 in the RAW 264.7 cells. Scale bar=20 μm. (B) Data points represent mean ± standard deviation from analysis of 3 separate images. $^{\#}p$<0.05 *vs.* blank control; ****p<0.0001 *vs.* LPS-stimulated cells, $^{\&\&}p$<0.01, $^{\&\&\&\&}p$<0.0001 *vs.* S or C. (C) Cells were cultured in T25 cell flasks and were pre-treated with S, C and SC (2.5 μg/mL) 1 h prior to LPS (1 μg/mL) for 24 h. The samples were then subjected to real-time PCR after RNA collection and cDNA synthesis. The mmu-miR-155-5p fold changes compared to untreated cells (Blank control). The data was expressed as the mean ± SEM. $^{\#}p$<0.05 *vs.* blank control; *p<0.05, ***p<0.001 *vs.* LPS stimulation.

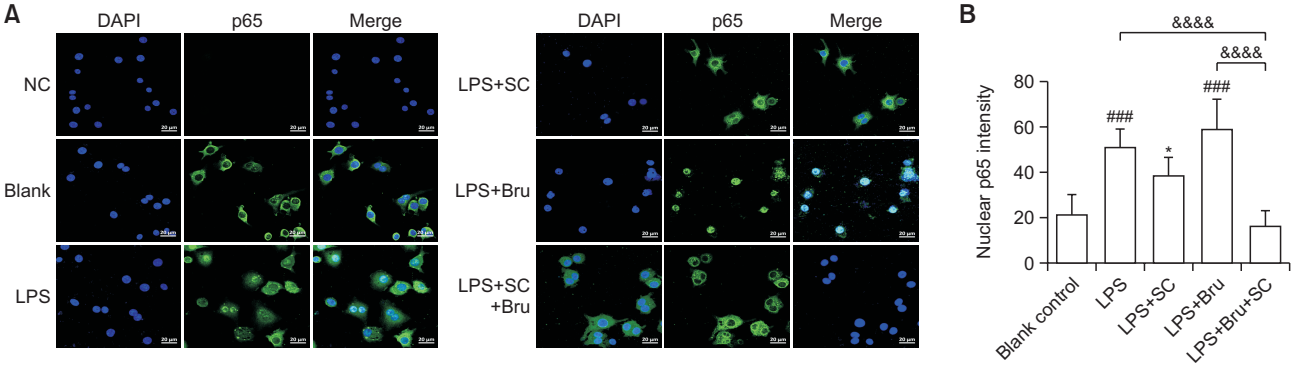

Fig. 6. The impact of Nrf2 blockage on the action of SC in inhibiting NFκB translocation. (A) RAW 264.7 cells were co-incubated with medium (Blank), SC (5 μg/mL), Bru (50 nM), SC (5 μg/mL) + Bru (50 nM) for 2 h prior to the stimulation of LPS (1 μg/mL) for another 30 min. Then the cells were prepared and subjected to fluorescent staining. Images were taken by using a confocal microscope with 40× magnification. Blue: DAPI in the nucleus, green: NFκB p65 in the RAW 264.7 cells. Scale bar=20 μm. Data points represent mean ± standard deviation from analysis of 3 separate images. (B) Data points represent mean ± standard deviation from analysis of 3 separate images. $^{\#\#\#}p$<0.001 *vs.* blank control; *p<0.05 *vs.* LPS-stimulated cells, $^{\&\&\&\&}p$<0.0001 *vs.* LPS+Bru.

the TLR4-TRAF-6-MAPK pathway were quantified by Western blot and compared that with the individual action.

LPS significantly increased the fold change of TLR4, TRAF6, p-JNK/JNK and p-cJUN/CJUN in RAW 264.7 cells compared to the untreated cells as shown in Fig. 7A-7D (p<0.05). S alone inhibited TLR-4 expression (p<0.01) and pJNK/JNK ratio (p<0.0001), whereas C alone showed a significant reduction in TLR4 expression (p<0.01), pJNK/JNK (p<0.0001) and p-c-JUN/c-JUN (p<0.0001). SC showed the most significant inhibition in all the key proteins (all p<0.01) in comparison to that of S and C, with the most significant activity in inhibiting p-JNK/JNK (p<0.0001).

A diagram explaining the mechanistic action of SC in reducing LPS-induced proinflammatory mediators is shown in Fig. 8.

DISCUSSION

CRS induced by bacteria or viral infection is one of the most critical events that involves a complex cellular cascade reaction and proinflammatory cytokine productions in the body. Previous studies have demonstrated C as a potential CSAIDs inhibiting CRS in viral infections (Sordillo and Helson, 2015; Liu and Ying, 2020). In line with previous findings, our results showed that C effectively reduced key proinflammatory me-

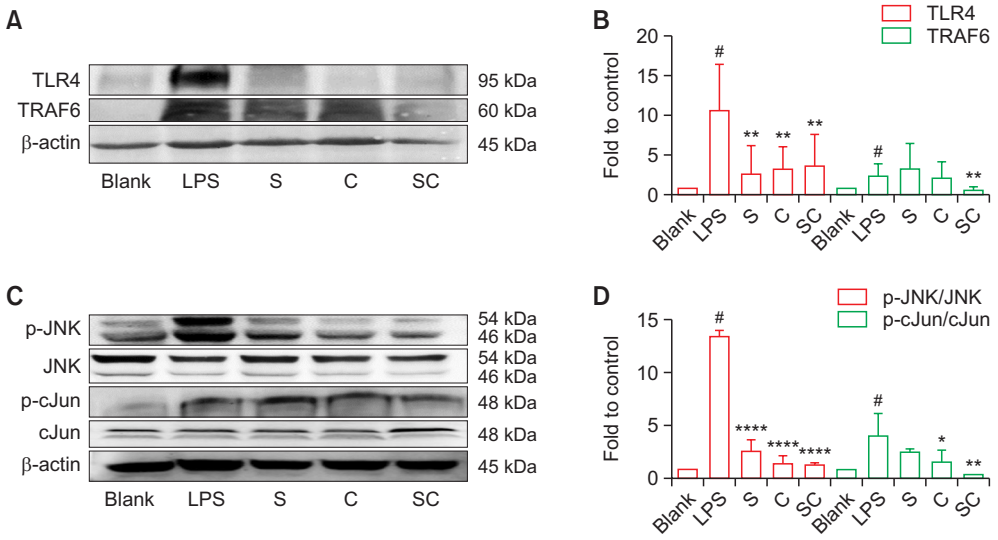

Fig. 7. SC downregulated key proteins and kinases in the TLR4-TRAF6-MAPK pathway in LPS and IFN-γ-stimulated RAW 264.7 cells (n=3). (A) Cells were cultured in T75 cell flasks and were pre-treated with S, C or SC 1 h prior to LPS (1 μg/mL) for 24 h. (B) Protein expression levels of TLR4 and TRAF-6 were analyzed by Western blot using whole protein extracts. (C) Cells were cultured in T75 cell flasks and were pre-treated with S, C or SC 1 h prior to LPS (1 μg/mL) for 40 min. (D) Protein expression levels of phosphorylated JNK (p-JNK), JNK, p-cJun, and cJun were analyzed by Western blot using whole protein extracts. All results (n=3) were expressed as the mean ± SEM, $^{\#}p<0.05$ *vs.* blank control; $^{*}p<0.05$, $^{**}p<0.01$, $^{****}p<0.0001$ *vs.* LPS-stimulated cells.

diators induced by LPS and IFN-γ, including NO (iNOS), TNF and IL-6, in RAW 264.7 and THP-1 cells. Moreover, our study has shown for the first time that C acted synergistically with 6-s and 10-s, in inhibiting key proinflammatory mediators via targeting TLR4/TRAF6/MAPK/NFκB signalings.

SC showed a greater and broader anti-cytokine activity compared to C in the cytokine array assay. It strengthened the downregulation of C on IL-6, TNF, macrophage inhibitory cytokine (MIC-1), IL-8, CXCL10 and MIG, and showed marked reductions on CXCL5,11 and MIP-3a in the cytokine array, while the effect of C alone was insignificant. CXCL family contains chemokines to recruit the first line of innate immune effector cells to sites of infection and inflammation in the initial stage of inflammation which contribute to the elimination of pathogens and contribute significantly to disease-associated processes, including tissue injury (Santos *et al*., 2020). The downregulation of CXCLs by SC indicates its potential capacity to regulate the activity of immune cells' activity and promote tissue repair in the infection-induced CRS (Gonzalez-Aparicio and Alfaro, 2019; KhalKhal *et al*., 2019). Previous studies have shown that C significantly decreased expressions of CXCLs, which regulated the activity of immune cells and inflammatory responses and promoted fibrosis in the lung after infection (Sordillo and Helson, 2015; Dai *et al*., 2018). Furthermore, a study from Jafarzadeh and Nemati (2018) suggested that ginger and its constituents may modulate the chemokines including CXCL10 and 11. Thus, although S did not show significant reduction of detected cytokines in present study, it synergistically enhanced the actions of C to broaden the action of SC to target a larger range of cytokines and chemokines.

To further explain the observed synergistic activity of SC in attenuating proinflammatory responses and cytokines, the individual and combined activity of S and C were explored in the LPS and IFN-γ induced proinflammatory molecular pathways. Our results indicated that the significant inhibition of proinflammatory cytokines by SC may be achieved via a multi-faceted signalling levels and their crosstalk in the cells. The bacterial and viral induced proinflammatory events start with recognizing invading microbial pathogens by TLR4 receptors and then signals through MyD88 to initiate multiple transcriptions (Dorrington and Fraser, 2019). In line with the previous studies (Zhou *et al*., 2014; Zhu *et al*., 2014), both S and C significantly decreased the expression of TLR4 as shown in the present study. However, the effect of SC on TLR4 was less significant than that of S or C which might be attributed to competing actions of S and C in the same receptor. Activation of TLR4 receptors leads to signal TRAF6 through MyD88 and results in (1) the activation of NFκB transcription and (2) the initiation of the MAPK pathway which leads to the transcription of AP1. Both transcription factors contribute to the production of proinflammatory cytokine production (Deng *et al*., 2013). The enhanced inhibition of SC on the secondary signal of TRAF6 in the TLR4-mediated pathways was observed, even though the effect of S and C was not significant. The individual action of 6-s and 10-s on TRAF6 was not clear, but C was shown to attenuate TRAF6 in Staphylococcus aureus-induced mouse mastitis at 20 μg/mL (Xu *et al*., 2020). A similar trend was observed in the downstream molecular targets that the activation of NFκB transcription and the phosphorylation of JNK and c-JUN were significantly supressed by SC. Individual 6-s and C have been shown to downregulate these two pathways (Li *et al*., 2012; Guimarães *et al*., 2013), which may add up to the combined action in SC.

We also examined the individual and combined effects of S and C on the expression of miR-155-5p. MiR-155-5p has been shown to upregulate rapidly upon the activation of NFκB transcription factor within 12 h (Mahesh and Biswas, 2019) which coordinates with NFkB axis for the proinflammatory signal amplification. Presently, miR-155-5p has been increasingly recognized as a novel therapeutic target for inflamma-

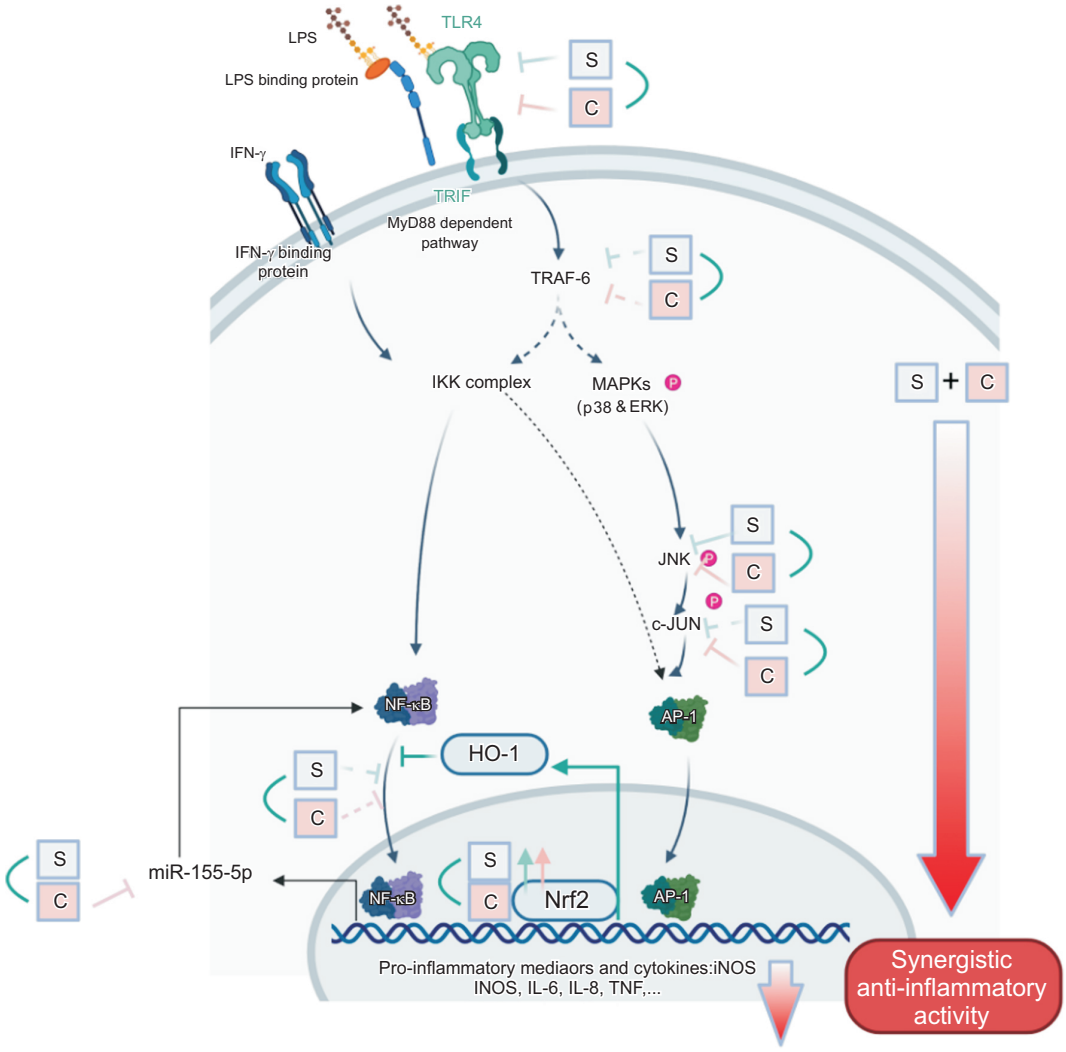

Fig. 8. Schematic diagram of the synergistic mechanism of SC in reducing LPS and IFN-γ-induced proinflammatory mediators. LPS activated TLR4 receptor on the cell membrane of RAW 264.7 cells, resulting in a cascade of activation of regulators including TRAF6-pJNK-p-c-JUN signaling and NFκB translocation which induced an excessive amount of proinflammatory cytokines released from cells. In addition, the upregulated miR-155-5p expression further activated the NFκB whereas Nrf2 induced HO-1 inhibited this pathway. Our results demonstrated that combined S and C at the synergistic dosage further strengthened their inhibitory activities in NFκB translocation, and downregulated TLR4/TRAF6/MAPK pathway. However, the anti-inflammatory action of SC was likely to be independent from the induction of Nrf2.

tory diseases (Gasparello *et al*., 2021). Our study revealed that C downregulated the increase of miR-155-5p induced by LPS, and this action was further strengthened in SC. Ma *et al*. (2017) demonstrated that C effectively protected mice from sepsis and cytokine productions which was associated to its reduction in miR-155. Our results supported this finding and further demonstrated that S synergizes C in further reducing the excessive release of miR-155-5p. This positive interaction may be attributed to miR-155 itself or indirect inhibitory activity in NFκB translocation.

Moreover, we have observed that SC magnified the induction of Nrf2 activity, contributing to the cellular anti-inflammatory system. Nrf2 has been well accepted as a basic leucine zipper transcription factor playing a key role in attenuating inflammation-associated pathogenesis related to the negative feedback of NFκB (Qin *et al*., 2015). During inflammation-mediated tissue damage, the activation of Nrf2 inhibited the production of proinflammatory mediators, including cytokines, chemokines, cell adhesion molecules, iNOS, etc. as evidenced by the fact that Nrf2-/- are more sensitive to inflammatory challenges and higher expression of cytokines in endotoxin-induced sepsis (Osburn *et al*., 2007; Hernandez *et al*., 2010; Thimmulappa *et al*., 2016). Many studies have shown that both C and 6-s upregulated Nrf2 and thus alleviated cytokine release and inflammation *in vitro* and *in vivo* (Boyanapalli *et al*., 2014; Chen *et al*., 2019; Bischoff-Kont and Fürst, 2021). Our present study showed that SC at 10.39-16.40 μg/mL amplified the upregulation of Nrf2 activity by over 10 folds. The protein expression of HO-1, the Nrf2-regulated down-stream anti-oxidant gene, was also upregulated by SC at 10 μg/mL. The magnified activation may come from (1) the additive effect of activation of Nrf2 by S and C; (2) the upstream modulator of the IκB kinase, (3) the

inhibitory effect of SC on NFκB translocation and its crosstalk with Nrf2. The upregulation of Nrf2 has also been suggested to impede the NFκB activity which then leads to a reduced proinflammatory response (Ahmed *et al*., 2017). To further examine the role of Nrf2 in the anti-inflammatory activity of SC, Bru (Nrf2 blocker) was co-incubated with SC for the observation of NFκB translocation. Our results suggested that SC at 5 μg/mL still significantly inhibited the translocation of p65 with the presence of the Nrf2 blocker. Thus, it appeared that the anti-inflammatory mechanism of SC was independent from the induction of Nrf2. Such action may be attributed to the low concentration required for the inhibition of NFκB pathway, as we noticed that the concentration required to induce Nrf2 by SC (>10 μg/mL) was much higher than the dosage required for the anti-inflammatory and anti-cytokine activity (IC_{50} values ≤6.63 μg/mL). A further mechanistic study in animal study is warranted to explore the crosstalk of these two pathways in the inflammatory condition to confirm the action of SC.

Taken together, the present study demonstrated a synergistic interaction of S and C in LPS and IFN-γ induced proinflammatory pathway which was associated with downregulating TLR4/TRAF/MAPK pathway and NFκB translocation. Our findings indicated that SC with its enhanced bioactivity and broader anti-inflammatory action may be useful as a novel therapeutic candidate for treating CRS and cytokine related inflammatory conditions.

CONFLICT OF INTEREST

The authors declare that the research was conducted in the absence of any commercial or financial relationships that could be construed as a potential conflict of interest. DL and HW are employees of Integria Healthcare (Australia) Pty Ltd which provided funding and in-kind support for the work as an Australian Research Council Linkage Project industry partner. A patent application (Australian Patent Application No. 2021902926) based in part on these results has been filed by Integria Healthcare (Australia) Pty Ltd naming XZ, GM, ML, DL HW, CGL and others as inventors.

ACKNOWLEDGMENTS

This study was supported by the Linkage Project from the Australian Research Council (ARC) grant (LP160101594). As a medical research institute, NICM Health Research Institute receives research grants and donations from foundations, universities, government agencies, individuals and industry. Sponsors and donors also provide untied funding for work to advance the vision and mission of the Institute.

REFERENCES

Ahmed, S. M. U., Luo, L., Namani, A., Wang, X. J. and Tang, X. (2017) Nrf2 signaling pathway: pivotal roles in inflammation. *Biochim. Biophys. Acta Mol. Basis Dis.* **1863**, 585-597.

Anand, P., Kunnumakkara, A. B., Newman, R. A. and Aggarwal, B. B. (2007) Bioavailability of curcumin: problems and promises. *Mol. Pharm.* **4**, 807-818.

Bischoff-Kont, I. and Fürst, R. (2021) Benefits of ginger and its constituent 6-Shogaol in inhibiting inflammatory processes. *Pharmaceuticals* **14**, 571.

Boyanapalli, S. S., Paredes-Gonzalez, X., Fuentes, F., Zhang, C., Guo, Y., Pung, D., Saw, C. L. L. and Kong, A.-N. T. (2014) Nrf2 knockout attenuates the anti-inflammatory effects of phenethyl isothiocyanate and curcumin. *Chem. Res. Toxicol.* **27**, 2036-2043.

Chen, F., Tang, Y., Sun, Y., Veeraraghavan, V. P., Mohan, S. K. and Cui, C. (2019) 6-shogaol, a active constiuents of ginger prevents UVB radiation mediated inflammation and oxidative stress through modulating NrF2 signaling in human epidermal keratinocytes (HaCaT cells). *J. Photochem. Photobiol., B* **197**, 111518.

Chousterman, B. G., Swirski, F. K. and Weber, G. F. (2017) Cytokine storm and sepsis disease pathogenesis. *Semin. Immunopathol.* **39**, 517-528.

Clark, I. A. (2007) The advent of the cytokine storm. *Immunol. Cell Biol.* **85**, 271-273.

Coperchini, F., Chiovato, L., Ricci, G., Croce, L., Magri, F. and Rotondi, M. (2021) The cytokine storm in COVID-19: further advances in our understanding the role of specific chemokines involved. *Cytokine Growth Factor Rev.* **58**, 82-91.

Cron, R. Q. (2021) COVID-19 cytokine storm: targeting the appropriate cytokine. *Lancet Rheumatol.* **3**, e236-e237.

D'Elia, R. V., Harrison, K., Oyston, P. C., Lukaszewski, R. A. and Clark, G. C. (2013) Targeting the "cytokine storm" for therapeutic benefit. *Clin. Vaccine immunol.* **20**, 319-327.

Dai, J., Gu, L., Su, Y., Wang, Q., Zhao, Y., Chen, X., Deng, H., Li, W., Wang, G. and Li, K. (2018) Inhibition of curcumin on influenza A virus infection and influenzal pneumonia via oxidative stress, TLR2/4, p38/JNK MAPK and NF-κB pathways. *Int. Immunopharmacol.* **54**, 177-187.

Deng, M., Scott, M. J., Loughran, P., Gibson, G., Sodhi, C., Watkins, S., Hackam, D. and Billiar, T. R. (2013) Lipopolysaccharide clearance, bacterial clearance, and systemic inflammatory responses are regulated by cell type-specific functions of TLR4 during sepsis. *J. Immunol.* **190**, 5152-5160.

Dorrington, M. G. and Fraser, I. D. (2019) NF-κB signaling in macrophages: dynamics, crosstalk, and signal integration. *Front. Immunol.* **10**, 705.

Gasparello, J., Finotti, A. and Gambari, R. (2021) Tackling the COVID-19 "cytokine storm" with microRNA mimics directly targeting the 3'UTR of pro-inflammatory mRNAs. *Med. Hypotheses* **146**, 110415.

Gonzalez-Aparicio, M. and Alfaro, C. (2019) Influence of interleukin-8 and neutrophil extracellular trap (NET) formation in the tumor microenvironment: is there a pathogenic role? *J. Immunol. Res.* **2019**, 6252138.

Guimarães, M. R., Leite, F. R. M., Spolidorio, L. C., Kirkwood, K. L. and Rossa, C., Jr. (2013) Curcumin abrogates LPS-induced pro-inflammatory cytokines in RAW 264.7 macrophages. Evidence for novel mechanisms involving SOCS-1, -3 and p38 MAPK. *Arch. Oral Biol.* **58**, 1309-1317.

Hernandez, M. L., Harris, B., Lay, J. C., Bromberg, P. A., Diaz-Sanchez, D., Devlin, R. B., Kleeberger, S. R., Alexis, N. E. and Peden, D. B. (2010) Comparative airway inflammatory response of normal volunteers to ozone and lipopolysaccharide challenge. *Inhal. Toxicol.* **22**, 648-656.

Islam, D., Lombardini, E., Ruamsap, N., Imerbsin, R., Khantapura, P., Teo, I., Neesanant, P., Gonwong, S., Yongvanitchit, K., Swierczewski, B. E., Mason, C. J. and Shaunak, S. (2016) Controlling the cytokine storm in severe bacterial diarrhoea with an oral Toll-like receptor 4 antagonist. *Immunology* **147**, 178-189.

Jablonska, E., Gorniak, P., Prusisz, W., Kiliszek, P., Szydlowski, M., Sewastianik, T., Bialopiotrowicz, M., Polak, A., Prochorec-Sobieszek, M., Szumera-Cieckiewicz, A., Warzocha, K. and Juszczynski, P. (2015) MiR-155 amplifies AKT and NFkB signaling by targeting multiple regulators of BCR signal in DLBCL. *Blood* **126**, 2455.

Jafarzadeh, A. and Nemati, M. (2018) Therapeutic potentials of ginger for treatment of Multiple sclerosis: a review with emphasis on its immunomodulatory, anti-inflammatory and anti-oxidative properties. *J. Neuroimmunol.* **324**, 54-75.

Jahrling, P. B., Hensley, L. E., Martinez, M. J., LeDuc, J. W., Rubins, K. H., Relman, D. A. and Huggins, J. W. (2004) Exploring the potential

of variola virus infection of cynomolgus macaques as a model for human smallpox. *Proc. Natl. Acad. Sci. U. S. A.* **101**, 15196-15200.
KhalKhal, E., Razzaghi, Z., Zali, H., Bahadorimonfared, A., Iranshahi, M. and Rostami-Nejad, M. (2019) Comparison of cytokine and gene activities in tissue and blood samples of patients with celiac disease. *Gastroenterol. Hepatol. Bed Bench* **12**, S108-S116.
Lehár, J., Krueger, A. S., Avery, W., Heilbut, A. M., Johansen, L. M., Price, E. R., Rickles, R. J., Short, G. F., 3rd, Staunton, J. E., Jin, X., Lee, M. S., Zimmermann, G. R. and Borisy, A. A. (2009) Synergistic drug combinations tend to improve therapeutically relevant selectivity. *Nat. Biotechnol.* **27**, 659-666.
Li, F., Nitteranon, V., Tang, X., Liang, J., Zhang, G., Parkin, K. L. and Hu, Q. (2012) *In vitro* antioxidant and anti-inflammatory activities of 1-dehydro-[6]-gingerdione, 6-shogaol, 6-dehydroshogaol and hexahydrocurcumin. *Food Chem.* **135**, 332-337.
Liu, Z. and Ying, Y. (2020) The inhibitory effect of curcumin on virus-induced cytokine storm and its potential use in the associated severe pneumonia. *Front. Cell Dev. Biol.* **8**, 479.
Ma, F. Y., Liu, F., Ding, L., You, M., Yue, H. M., Zhou, Y. J. and Hou, Y. Y. (2017) Anti-inflammatory effects of curcumin are associated with down regulating microRNA-155 in LPS-treated macrophages and mice. *Pharm. Biol.* **55**, 1263-1273.
Mahesh, G. and Biswas, R. (2019) MicroRNA-155: a master regulator of inflammation. *J. Interferon Cytokine Res.* **39**, 321-330.
Meng, Q. F., Tian, R., Long, H., Wu, X., Lai, J., Zharkova, O., Wang, J. W., Chen, X. and Rao, L. (2021) Capturing cytokines with advanced materials: a potential strategy to tackle COVID-19 cytokine storm. *Adv. Mater.* **33**, e2100012.
Miao, Y., Zhao, S., Gao, Y., Wang, R., Wu, Q., Wu, H. and Luo, T. (2016) Curcumin pretreatment attenuates inflammation and mitochondrial dysfunction in experimental stroke: the possible role of Sirt1 signaling. *Brain Res. Bull.* **121**, 9-15.
Miossec, P. (2020) Synergy between cytokines and risk factors in the cytokine storm of COVID-19: does ongoing use of cytokine inhibitors have a protective effect? *Arthritis Rheumatol.* **72**, 1963-1966.
Murthy, S. and Lee, T. C. (2021) IL-6 blockade for COVID-19: a global scientific call to arms. *Lancet Respir. Med.* **9**, 438-440.
Osburn, W. O., Karim, B., Dolan, P. M., Liu, G., Yamamoto, M., Huso, D. L. and Kensler, T. W. (2007) Increased colonic inflammatory injury and formation of aberrant crypt foci in Nrf2-deficient mice upon dextran sulfate treatment. *Int. J. Cancer* **121**, 1883-1891.
Pan, M. H., Hsieh, M. C., Hsu, P. C., Ho, S. Y., Lai, C. S., Wu, H., Sang, S. and Ho, C. T. (2008) 6-Shogaol suppressed lipopolysaccharide-induced up-expression of iNOS and COX-2 in murine macrophages. *Mol. Nutr. Food Res.* **52**, 1467-1477.
Qin, S., Du, R., Yin, S., Liu, X., Xu, G. and Cao, W. (2015) Nrf2 is essential for the anti-inflammatory effect of carbon monoxide in LPS-induced inflammation. *Inflamm. Res.* **64**, 537-548.
Santos, I., Colaço, H. G., Neves-Costa, A., Seixas, E., Velho, T. R., Pedroso, D., Barros, A., Martins, R., Carvalho, N., Payen, D., Weis, S., Yi, H. S., Shong, M. and Moita, L. F. (2020) CXCL5-mediated recruitment of neutrophils into the peritoneal cavity of Gdf15-deficient mice protects against abdominal sepsis. *Proc. Natl. Acad. Sci. U. S. A.* **117**, 12281-12287.
Saw, C. L. L., Huang, Y. and Kong, A.-N. (2010) Synergistic anti-inflammatory effects of low doses of curcumin in combination with polyunsaturated fatty acids: docosahexaenoic acid or eicosapentaenoic acid. *Biochem. Pharmacol.* **79**, 421-430.
Sordillo, P. P. and Helson, L. (2015) Curcumin suppression of cytokine release and cytokine storm. A potential therapy for patients with Ebola and other severe viral infections. *In Vivo* **29**, 1-4.
Soy, M., Keser, G., Atagündüz, P., Tabak, F., Atagündüz, I. and Kayhan, S. (2020) Cytokine storm in COVID-19: pathogenesis and overview of anti-inflammatory agents used in treatment. *Clin. Rheumatol.* **39**, 2085-2094.
Thimmulappa, R. K., Lee, H., Rangasamy, T., Reddy, S. P., Yamamoto, M., Kensler, T. W. and Biswal, S. (2016) Nrf2 is a critical regulator of the innate immune response and survival during experimental sepsis. *J. Clin. Invest.* **116**, 984-995.
Tisoncik, J. R., Korth, M. J., Simmons, C. P., Farrar, J., Martin, T. R. and Katze, M. G. (2012) Into the eye of the cytokine storm. *Microbiol. Mol. Biol. Rev.* **76**, 16-32.
Wang, W., Liu, X., Wu, S., Chen, S., Li, Y., Nong, L., Lie, P., Huang, L., Cheng, L., Lin, Y. and He, J. (2020) Definition and risks of cytokine release syndrome in 11 critically ill COVID-19 patients with pneumonia: analysis of disease characteristics. *J. Infect. Dis.* **222**, 1444-1451.
World Health Organization (2020) The Top 10 Causes of Death. Available from: https://www.who.int/news-room/fact-sheets/detail/the-top-10-causes-of-death/.
Xu, J., Jia, Z., Chen, A. and Wang, C. (2020) Curcumin ameliorates Staphylococcus aureus-induced mastitis injury through attenuating TLR2-mediated NF−κB activation. *Microb. Pathog.* **142**, 104054.
Yokota, S. (2003) Influenza-associated encephalopathy--pathophysiology and disease mechanisms. *Nihon Rinsho* **61**, 1953-1958.
Yuen, K. and Wong, S. (2005) Human infection by avian influenza A H5N1. *Hong Kong Med. J.* **11**, 189-199.
Zhou, L., Qi, L., Jiang, L., Zhou, P., Ma, J., Xu, X. and Li, P. (2014) Antitumor activity of gemcitabine can be potentiated in pancreatic cancer through modulation of TLR4/NF-κB signaling by 6-shogaol. *AAPS J.* **16**, 246-257.
Zhou, X., Afzal, S., Wohlmuth, H., Münch, G., Leach, D., Low, M. and Li, C. G. (2022a) Synergistic anti-inflammatory activity of ginger and turmeric extracts in inhibiting lipopolysaccharide and interferon-γ-induced proinflammatory Mediators. *Molecules* **27**, 3877.
Zhou, X., Münch, G., Wohlmuth, H., Afzal, S., Kao, M., Al-Khazaleh, A., Low, M., Leach, D. and Li, C. G. (2022b) Synergistic inhibition of pro-inflammatory pathways by ginger and turmeric extracts in RAW 264.7 cells. *Front. Pharmacol.* **13**, 818166.
Zhou, X., Razmovski-Naumovski, V., Kam, A., Chang, D., Li, C., Bensoussan, A. and Chan, K. (2017) Synergistic effects of Danshen (Salvia Miltiorrhizae Radix et Rhizoma) and Sanqi (Notoginseng Radix et Rhizoma) combination in angiogenesis behavior in EAhy 926 cells. *Medicines* **4**, 85.
Zhou, X., Razmovski-Naumovski, V., Kam, A., Chang, D., Li, C. G., Chan, K. and Bensoussan, A. (2019) Synergistic study of a Danshen (Salvia Miltiorrhizae Radix et Rhizoma) and Sanqi (Notoginseng Radix et Rhizoma) combination on cell survival in EA.hy926 cells. *BMC Complement. Altern. Med.* **19**, 50.
Zhou, X., Seto, S. W., Chang, D., Kiat, H., Razmovski-Naumovski, V., Chan, K. and Bensoussan, A. (2016) Synergistic effects of Chinese herbal medicine: a comprehensive review of methodology and current research. *Front. Pharmacol.* **7**, 201.
Zhu, H.-t., Bian, C., Yuan, J.-c., Chu, W.-h., Xiang, X., Chen, F., Wang, C.-s., Feng, H. and Lin, J.-k. (2014) Curcumin attenuates acute inflammatory injury by inhibiting the TLR4/MyD88/NF-κB signaling pathway in experimental traumatic brain injury. *J. Neuroinflammation* **11**, 59.